Acta Oceanol. Sin., 2018, Vol. 37, No. 7, P. 20–27
DOI: 10.1007/s13131-018-1241-1
http://www.hyxb.org.cn
E-mail: hyxbe@263.net

Methane seepage intensities traced by sulfur isotopes of pyrite and gypsum in sediment from the Shenhu area, South China Sea

ZHANG Mei[1]*, LU Hongfeng[2], GUAN Hongxiang[1, 3], LIU Lihua[1], WU Daidai[1], WU Nengyou[3, 4]

[1] Key Laboratory of Gas Hydrate, Guangzhou Institute of Energy Conversion, Chinese Academy of Sciences, Guangzhou 510640, China

[2] Guangzhou Marine Geological Survey, Guangzhou 510760, China

[3] Laboratory for Marine Mineral Resources, Qingdao National Laboratory for Marine Science and Technology, Qingdao 266061, China

[4] Key Laboratory of Gas Hydrate, Qingdao Institute of Marine Geology, Ministry of Land and Resources, Qingdao 266071, China

Received 24 July 2017; accepted 20 October 2017

Abstract

The northern slope of the South China Sea is a gas-hydrate-bearing region related to a high deposition rate of organic-rich sediments co-occurring with intense methanogenesis in subseafloor environments. Anaerobic oxidation of methane (AOM) coupled with bacterial sulfate reduction results in the precipitation of solid phase minerals in seepage sediment, including pyrite and gypsum. Abundant aggregates of pyrites and gypsums are observed between the depth of 667 and 850 cm below the seafloor (cmbsf) in the entire core sediment of HS328 from the northern South China Sea. Most pyrites are tubes consisting of framboidal cores and outer crusts. Gypsum aggregates occur as rosettes and spheroids consisting of plates. Some of them grow over pyrite, indicating that gypsum precipitation postdates pyrite formation. The sulfur isotopic values (δ^{34}S) of pyrite vary greatly (from –46.6‰ to –12.3‰ V-CDT) and increase with depth. Thus, the pyrite in the shallow sediments resulted from organoclastic sulfate reduction (OSR) and is influenced by AOM with depth. The relative high abundance and δ^{34}S values of pyrite in sediments at depths from 580 to 810 cmbsf indicate that this interval is the location of a paleo-sulfate methane transition zone (SMTZ). The sulfur isotopic composition of gypsum (from –25‰ to –20.7‰) is much lower than that of the seawater sulfate, indicating the existence of a ^{34}S-depletion source of sulfur species that most likely are products of the oxidation of pyrites formed in OSR. Pyrite oxidation is controlled by ambient electron acceptors such as MnO_2, iron (III) and oxygen driven by the SMTZ location shift to great depths. The δ^{34}S values of gypsum at greater depth are lower than those of the associated pyrite, revealing downward diffusion of ^{34}S-depleted sulfate from the mixture of oxidation of pyrite derived by OSR and the seawater sulfate. These sulfates also lead to an increase of calcium ions from the dissolution of calcium carbonate mineral, which will be favor to the formation of gypsum. Overall, the mineralogy and sulfur isotopic composition of the pyrite and gypsum suggest variable redox conditions caused by reduced seepage intensities, and the pyrite and gypsum can be a recorder of the intensity evolution of methane seepage.

Key words: pyrite tube, authigenic gypsum, sulfur isotopes, methane seepage, northern South China Sea

Citation: Zhang Mei, Lu Hongfeng, Guan Hongxiang, Liu Lihua, Wu Daidai, Wu Nengyou. 2018. Methane seepage intensities traced by sulfur isotopes of pyrite and gypsum in sediment from the Shenhu area, South China Sea. Acta Oceanologica Sinica, 37(7): 20–27, doi: 10.1007/s13131-018-1241-1

1 Introduction

Methane seepage is a widely observed phenomenon along continental margins worldwide (e.g., Campbell, 2006; Suess, 2014). Anaerobic oxidation of methane (AOM) driven by sulfate from seawater is the key process in consuming methane mediated by a consortium of methanotrophic archaea and sulfate-reducing bacteria at seeps, according to Eq. (1) (Boetius et al., 2000; Orphan et al., 2001; Wegener et al., 2015). This process results in precipitation of sulfide and eventual transformation into pyrite in the seep sediments (Peckmann et al., 2001; Zhang et al., 2014a; Lin et al., 2016b, c, d).

$$CH_4 + SO_4^{2-} \rightarrow HS^- + HCO_3^- + H_2O. \quad (1)$$

However, pyrite formation can also result from remineralization of organic matter by microbial sulfate reduction (OSR) (Eq. (2)) that occurs during early sediment diagenesis (e.g., Berner, 1980; Jørgensen, 1982; Canfield, 1991; Mazumdar et al., 2012).

$$2(CH_2O) + SO_4^{2-} \rightarrow H_2S + 2HCO_3^-. \quad (2)$$

Pyrite derived from AOM exhibits high δ^{34}S values compared with pyrite resulting from OSR acting as an indicator for methane release in marine sediments (Jørgensen et al., 2004; Neretin

Foundation item: The Qingdao National Laboratory for Marine Science and Technology under contract No. QNLM2016ORP0210; the National Natural Science Foundation of China under contract Nos 41306061, 41473080 and 41376076; the Scientific Cooperative Project by China National Petroleum Corporation and Chinese Academic of Sciences under contract No. 2015A- 4813.
*Corresponding author, E-mail: zhangmei@ms.giec.ac.cn

et al., 2004; Lim et al., 2011; Peketi et al., 2012, 2015; Borowski et al., 2013). These positive $\delta^{34}S$ values have been interpreted to reflect enhanced uprising of methane from dissociation of methane hydrate (e.g., Jørgensen al., 2004; Neretin et al., 2004; Peketi et al., 2012, 2015; Pirlet et al., 2012; Borowski et al., 2013; Wang et al., 2015; Lin et al., 2016b, c, d).

Gypsum is another authigenic mineral in marine sediments associated with gas hydrate (Sassen et al., 2004; Wang et al., 2004; Chen et al., 2007; Pierre et al., 2012, 2014, 2017; Kocherla et al., 2013; Novikova et al., 2015; Lin et al., 2016a, c), even though gypsum is undersaturated in seawater (Pirlet et al., 2010). Some authors have attributed this to reoxidized sulfide minerals promoted by the bioirrigation and burrowing activity of benthic seep fauna (Pierre et al., 2012). However, the origin of gypsum and its relationship with pyrite and gas hydrate remain unclear. In recent articles, Lin et al. (2016c) presented research on gypsum in the gas hydrate bearing sediments in northern South China Sea (SCS). Some authors also have reported occurrences of pyrite and authigenic gypsum in gas-hydrate-bearing sediments (Pierre, 2017; Lin et al., 2016a). These authors proposed that authigenic gypsum precipitated in the sulfate–methane transition zone (SMTZ), wherein pore water sulfate resulted from the mixing of the ^{34}S-rich residual seawater sulfate and sulfate derived from pyrite oxidation. Here, we present detailed microscopic observations and sulfur-stable isotope composition of authigenic pyrite and gypsum from seepage sediments of the SCS to determine the links between methane seepage intensities and precipitation of sulfate and sulfide minerals in the sediment. These results not only help us understand the formation of these minerals but also confirm the variations in seepage intensity controlled by gas hydrate dissolution.

2 Geological setting

The SCS is one of the largest marginal seas in the western Pacific Ocean and lies at the junction of three plates: the Eurasian plate, the Pacific plate, and the Indo-Australian plate (Fig. 1). The SCS exhibits a complex and unique tectono-sedimentary framework (McDonnell et al., 2000; Wang et al., 2006). The northern slope of the SCS is a passive continental margin that has been shaped by three main tectonic stages since the Cenozoic: the Paleocene rift stage, the Eocene thermal subsidence stage, and the Neotectonic movement stage (Zhu et al., 2012). Here, the complex fractures, faults and diapirs are widely developed in the subsurface and can serve as pathways for hydrocarbon migration.

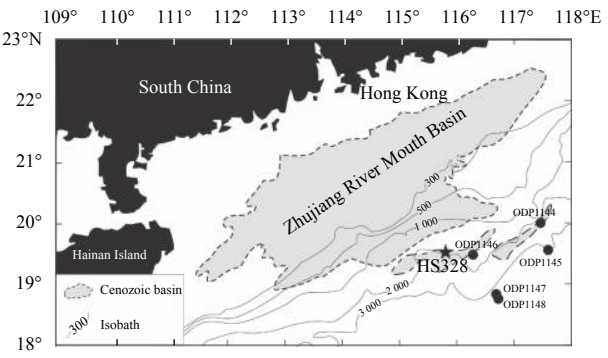

Fig. 1. Sampling location of HS328 in the Shenhu area, northern South China Sea (modified from Lu et al., 2007). The point of five star is the sampling location of HS328 core sediment and the dark circles are the locations of the ocean drilling program drills.

Investigations of this area have revealed great potential for gas hydrate and petroleum exploration (McDonnell et al., 2000; Wang et al., 2006; Jiang et al., 2008; Wu et al., 2010). Previous studies have indicated a high deposition rate in this marine area, ranging from 4 000 to 7 000 m of sediments during the Cenozoic era, along with high concentrations of organic matter. The heat flow ranges from 74 to 78 mW/m^2 and the geothermal gradient is approximately 45 to 67.7 °C/km, representing favorable conditions for the occurrence of gas hydrates (Wu et al., 2007). In addition, well-developed bottom-simulating reflectors as evidence for widespread hydrate occurrence and abundant seep carbonates have been discovered in the Shenhu area (Han et al., 2008; Ge et al., 2010; Tong et al., 2013; Lu et al., 2015; Guan et al., 2016b). In June 2007, a gas hydrate sample was successfully drilled for the first time in the Shenhu area (Liu et al., 2012). These observations confirm that gas hydrates are common in the northern SCS, particularly in the Shenhu area.

3 Sample collection and analysis

The studied piston core was recovered at site HS328 in the Shenhu area during a cruise on the R/V *Haiyang Sihao* in 2006 (Fig. 1). The water depth is 1 378 m, and the length of the core is 8.50 m. After retrieval, the core was cut into sections at an interval of 0.7 m from the top to the bottom, and the top 20 cm of sediments in each section were prepared for measuring headspace gas and extracting pore water onboard. The shipboard analysis of methane and sulfate followed the procedures of Cheng and Lu, (2005).

For this study, half of the sample was taken and packed in a Ziploc plastic material at intervals of 20 cm from the top to the bottom. Samples were dried at 40°C in a dry oven for 24 h, then soaked in distilled water for 24 h, rinsed gently with distilled water with a 0.063 mm sifter, and redried in an air-dry oven. Pyrite and gypsum aggregates from the coarse fraction were identified with a binocular microscope, hand-picked and weighed. The mass fraction of pyrite and gypsum in the host sediment was used to estimate the overall content of these two minerals.

Morphological descriptions of microscopic features were obtained by scanning electron microscope (SEM). SEM samples were prepared by dispersing powders on samples stages and then they were lightly Au-coated. SEM observation was performed at the Guangzhou Institute of Energy Conversion, Chinese Academy of Sciences (GIEC, CAS), using a Hitachi S4800 SEM equipped with an electron back-scattering system and energy dispersive X-ray spectroscopy (EDS) capabilities to determine the solid-phase composition.

For sulfur stable isotope analysis, gypsum samples were purified by $BaSO_4$ precipitation. The extraction process was performed according to Longinelli and Flora (2007). Approximately 100 mg of gypsum was crushed and ground into powder and dissolved in double-distilled water. The solution was filtered to eliminate insoluble impurities before an acidified (using 1 mol/dm^3 HCl) $BaCl_2$ solution was added. Then, the $BaSO_4$ precipitate was filtered and washed with double-distilled water and dried overnight at 120°C.

The stable sulfur isotopes of the pyrite and gypsum were measured using a Delta V Plus mass spectrometer coupled to an elemental analyzer (EA-IRMS) at the State Key Laboratory of Biogeology and Environmental Geology, China University of Geosciences (BGEG, CUG) in Wuhan. Before the test, $BaSO_4$ was oxidized to SO_2 using an excess of V_2O_5 at 980°C. Pyrite was converted to SO_2 by combustion using CuO. All results are reported here in standard delta notation as per mil deviations from the Vienna-defined Canyon Diablo Troilite (V-CDT). Measurement er-

rors of approximately 0.2‰ (1r) were calculated from replicate analyses of the International Atomic Energy Agency (IAEA) international standards: IAEA S_1 (–0.3‰), IAEA S_2 (+22.7‰), and IAEA S_3 (–32.3‰).

$$\delta^{34}S = \left[\left({}^{34}S/{}^{32}S\right)_{sample} / \left({}^{34}S/{}^{32}S\right)_{V-CDT} - 1\right] \times 10^3. \quad (3)$$

4 Results

The distributions of sulfate and methane concentrations in the pore water of core sediments are shown in Fig. 2a. The concentration of sulfate ions steadily decrease from top to bottom, from 27.14 to 5.82 mmol/L. The methane concentration is low and changes slightly from 11.48 to 17.59 μg/L. The contents of total organic carbon (TOC) in the bulk sediment range from 0.92% to 1.93%, with an average value of 1.46% (Fig. 2b). Layers shallower than 500 cm have organic carbon contents that are relatively low, with an average value of 1.33%. Layers deeper than 500 cm are relatively high, with an average value of 1.60% (Fig. 2b).

The contents of pyrite and gypsum in the bulk sediment are shown in Figs 2c and d. The content of pyrite increases with depth, ranging from 0.000 4% to 0.129%. Pyrite content is very low, with an average of 0.007% above 355 cm. Between 368 and 650 cm, the average pyrite content is 0.02%. The highest content of pyrite is from 667 to 850 cm, with an average of 0.057% and a peak of 0.11% at 705 cm (Fig. 2c). Therefore, the contents of TOC and pyrite in the sediments increased with depth, but the pyrite content increased quickly. The content of gypsum is higher than pyrite, and the average content of gypsum is 0.095% in the core sediments; the highest content (0.89%) is found in the same layer as that of pyrite (705 cm) (Fig. 2d).

In core sediment of HS328, pyrite and gypsum are two major authigenic minerals. Most hand-picked pyrite aggregates are yellow or black in color and rod-like in shape (Figs 3a to c). In addition, pyrite aggregates formed in chambers of foraminiferan tests. Both pyrite types consist of clustered framboids. Pyrite tubes vary mainly from 2 to 7 mm in length and 0.2 to 0.6 mm in diameter, whereas some of the tubes are large, with a length of 25 mm and a diameter of 3 mm, particularly at a depth of 700 cm. Most rod-like pyrite aggregates from HS328 cores show two main crystal habits: framboids (Figs 4a, b, d and e) and euhedral pyrite crystals (Figs 4c and e). The pyrite becomes longer and darker with increasing sediment depth (Figs 3a–c). Framboid is the main observed textural form in the tube pyrite aggregations (Figs 4a–e). Framboidal pyrite usually consists of octahedral pyrite microcrystals. Some of the framboids are observed to be packed closely together by the disordered crystal, whereas others are scattered (Figs 4a–e).

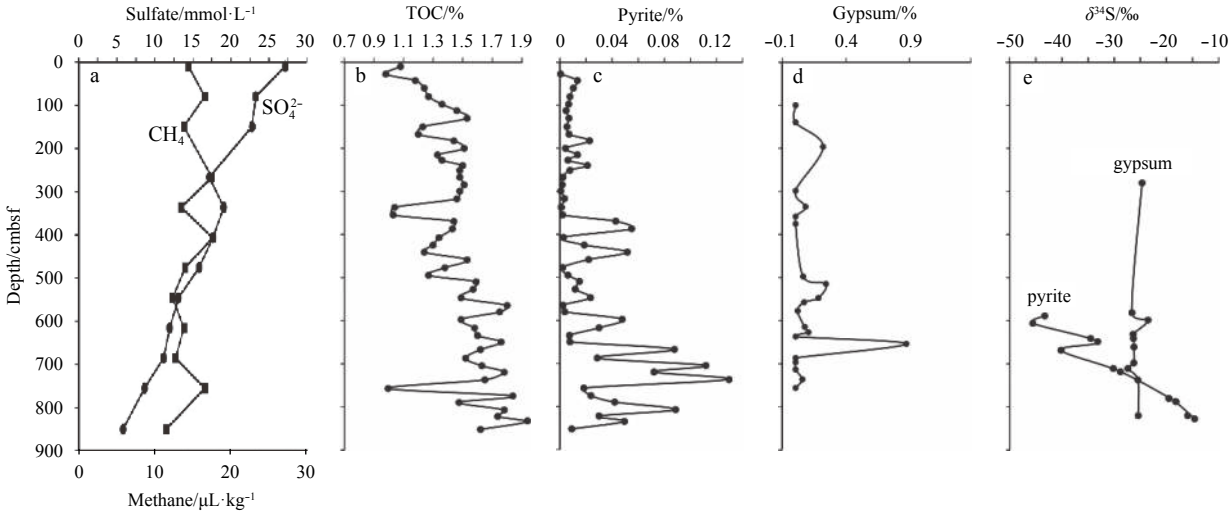

Fig. 2. Pore water and sediment geochemistry of site HS328. a. Profiles of interstitial-dissolved sulfate and methane, b. content of total organic carbon in the bulk sediment, c. content of the pyrite in the bulk sediment, d. content of the gypsum in the bulk sediment, and e. sulfur isotopic composition of hand-picked pyrite and gypsum.

Gypsum is another main authigenic mineral. Most gypsum aggregates appear in various shapes, including spherules, dumbbells, and rosettes, which are 1–3 mm in diameter (Figs 3e and f). Gypsum rosettes consist of lenticular, plate-shaped crystals, which are either a roughly orientated radial pattern (Figs 4e and g) or orientated parallel resulting in a stacked pattern (Figs 4f, h and i). Some of the pyrite and gypsum aggregates also show intergrowth relationships (Figs 3d and 4e), occasionally to a point that pyrite is completely engulfed by gypsum (Fig. 3d), indicating that gypsum precipitation postdated pyrite formation.

The sulfur isotope values of pyrite and gypsum are presented in Fig. 2e. The $\delta^{34}S$ values of pyrite vary from –46.6‰ to –12.3‰ and the values increase with depth, peaking at a interval of 820–830 cm with a $\delta^{34}S$ value of –12.3‰. The $\delta^{34}S$ values of gypsum aggregates reveal a narrow range from –25.0‰ to –20.7‰. The sulfur isotopes of gypsum show a stable value that does not vary with depth.

5 Discussion

5.1 *Authigenic pyrite indicating paleo-SMTZ*

The SMTZ is the most intense sulfate and methane consumption layer, wherein methane and sulfate are generally consumed completely. The depth of the SMTZ can reflect the possibility of the occurrence of gas hydrates at greater depths. A shallow SMTZ is associated with increased methane flux intensity and high rates

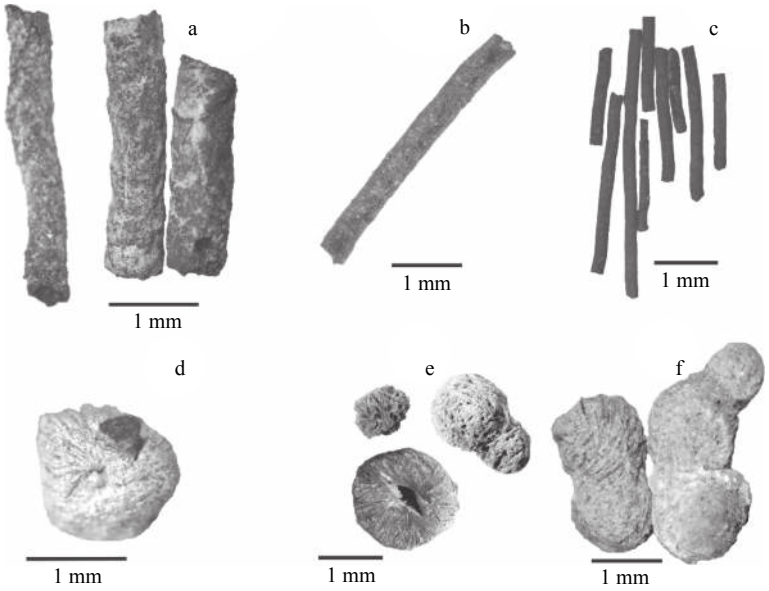

Fig. 3. Macroscopic observations of the authigenic pyrite and gypsum aggregates. a–c. Pyrite tubes, d. gypsum that apparently overgrew in a pyrite tube, e. typical gypsum rosette, spherule, and f. gypsum dumbbell.

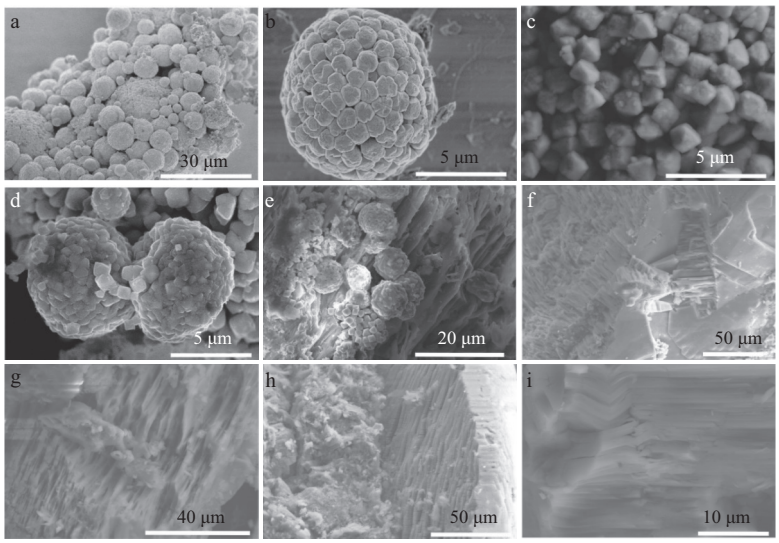

Fig. 4. Scanning electron microscope observations of pyrite and gypsum aggregates. a. Tubular pyrite showing agglomerates of framboids, b. spherical framboidal pyrite, c. octahedral and second pyrite crystals, d. spherical framboids, e. pyrite framboids surrounded by gypsum, f. gypsum rosette consisting of plate-like gypsum crystals, g. gypsum partly in dissolution, h. gypsum rosette consisting of lenticular gypsum crystals, and i. plate-like gypsum.

of AOM, which will cause an obvious decrease in the fractionation of sulfur isotopes between the precipitation of authigenic sulfide minerals and seawater sulfate within the SMTZ (Canfield et al., 2010; Sim et al., 2011; Peketi et al., 2012; Antler et al., 2013; Leavitt et al., 2013; Deusner et al., 2014; Zhang et al., 2014b; Lin et al., 2016a, b, d). However, the methane and sulfate concentrations of HS328 are not consumed completely. Some of methane reaches the surface sediments (Fig. 2a). Thus, the AOM-driven sulfate reduction is not active to date, and the high content of pyrite in the HS328 core sediments was driven by intense seepage and AOM in the past. The interval of high pyrite contents with high δ^{34}S values (667–850 cm) could serve as a proxy for the location of a paleo-SMTZ.

5.2 *Formation of authigenic pyrite*

The formation of authigenic pyrite in marine sediments is mainly influenced by several factors, such as organic matter content, methane flux, sulfate supply, and active iron content. H_2S generated from sulfate reduction driven by organic matter or methane is the main factor controlling the content of pyrite because it will precipitate as FeS and then transform to authigenic pyrite via several possible pathways in anoxic marine sediments (e.g., Butler et al., 2004; Neretin et al., 2004, and references therein). If a flux of methane from deep sediment exists, it would result in the additional production of H_2S that precipitates anomalously high concentrations of authigenic pyrites preserved in the sedimentary column.

Most pyrite aggregates from sediments of core HS328 display a distinct tube- or rod-like shape, similar to occurrences in other methane-rich areas, such as the northern SCS (e.g., Xie et al., 2013; Zhang et al., 2014a; Lin et al., 2016a, d) and the Gulf of Mexico (Sassen et al., 2004). Several studies show that tubular and rod-like pyrite morphologies can act as microchannels for methane migration (Lu et al., 2007; Lin et al., 2016a, d), but we consider this condition as a pseudomorphous appearance of bacterium (Sassen et al., 2004; Zhang et al., 2014a).

Usually, framboids are considered to have formed through rapid nucleation and relatively rapid crystal growth via mackinawite (FeS) and/or greigite (Fe_3S_4) intermediates under extremely high supersaturation (Wilkin and Barnes, 1996; Butler and Rickard, 2000; Ohfuji and Rickard, 2005; Rickard and Luther, 2007). This process removes most of sulfide and iron from the initial environment (Ohfuji and Rickard, 2005; Rickard, 2015). When pyrite seed crystals are present, continuous pyrite growth will be passing through AOM within the SMTZ if methane is supplied continually in a seepage setting. Most of the pyrite aggregates in this study are framboidal core and outer crust in the paleo-SMTZ, which means enhanced methane supply through AOM to allow the continuous growth of pyrite after framboid precipitation.

In addition, the high ^{34}S depletion of pyrite (–46.6‰ to –32.9‰) in the shallow sediment of core HS328 (above 667 cmbsf) indicates that the mineralization of OSR is the main process in precipitating pyrite (Canfield and Thamdrup, 1994; Habicht and Canfield, 2001). The high decomposition rate of organic matter, which is driven by OSR, results from the relatively low content of organic matter in the shallow sediments. The sharp increase in the $\delta^{34}S$ value of pyrite between 667 and 850 cmbsf revealed that the ^{34}S-enriched hydrogen sulfide was supplied by AOM. The rapid rate of AOM has been considered as the cause of reduced fractionation between sulfate and hydrogen sulfide and production of the relatively high $\delta^{34}S$ values of pyrite preserved in the SMTZ sediments.

5.3 *Possible sources and formation processes of gypsum*

Gypsum is a common evaporitic mineral. Although the sulfate concentration in seawater is not high enough to form gypsum, it is still commonly reported in marine sediments, especially in gas hydrate sedimentary environments (e.g., Wang et al., 2004; Sassen et al., 2004; Chen et al., 2007; Pirlet et al., 2012; Kocherla, 2013; Lin et al., 2016a, c; Pierre et al., 2012, 2017).

The morphological characteristics of the gypsum crystals in Core HS328 are consistent with an authigenic origin. The gypsum in the study core are rosette aggregates between 0.1 and 2.0 cm (Figs 3d to f), and several types of authigenic gypsum are also found near the sites of the northern SCS (e.g., Lin et al., 2016a, c). In addition, the ^{34}S depletion of gypsum (from –25.0‰ to –20.7‰ V-CDT) in the entire core sediment excludes the possibility of residual pore water sulfate that has relatively high ^{34}S values forming gypsum in the course of drilling or afterwards. In addition, the $\delta^{34}S$ values of gypsum are lower than those of pyrite at great depths, indicating that it does not result from oxidation of the associated pyrite in the course of drilling or afterwards (Lin et al., 2016a). The oxidation of pore water H_2S, which has a low $\delta^{34}S$ value (Jørgensen et al., 2004), and the oxidation of H_2S produces up to 18‰ sulfur isotope enrichment in the sulfate (Böttcher and Thamdrup, 2001; Böttcher et al., 2005; Habicht et al., 1998). Besides, recent studies of $\delta^{34}S$ and $\delta^{18}O$ of gypsum and the mass balance consideration of sediment pore water in the northern SCS also excluded that gypsum precipitated from sediment pore waters H_2S in the course of drilling or afterwards (Lin et al., 2016a, c).

Generally, seawater sulfate ($\delta^{34}S$ = 20.3‰; Faure, 1986) is a major source of precipitation of sulfate minerals in marine environments, although seawater is unsaturated in terms of the precipitation of gypsum. Oxidation of sulfide minerals is a possible source of elevated sulfate concentration in the pore water (Balci et al., 2007) although oxygen would be consumed by aerobic respiration in shallow subsurface sediment. Some other electron acceptors such as MnO_2 and iron (III) drive the oxidization of sulfide under anaerobic conditions in deep subsurface sediments (Schippers and Jørgensen, 2001). In addition, the oxidization of sulfides in deep subsurface sediment is generally associated with bioturbation, bottom currents, or seismic mixing (Pirlet et al., 2010).

Compared with modern seawater sulfate (+20.3‰), the sulfur isotopic composition of gypsum at core HS328 (–25.0‰ to –20.7‰) reflects a significant depletion in ^{34}S, revealing the existence of a ^{34}S-depleted source of sulfur species that most likely dissolved hydrogen sulfide or sedimentary sulfide minerals. Pirlet et al. (2010) have attributed ^{34}S-depleted gypsum to the oxidation of the ^{34}S-depleted pyrite in the sediment as sulfate derived from pyrite oxidation exhibits a similar sulfur isotope composition as pyrite (e.g., Balci et al., 2007). At Site HS328, pyrite and gypsum are the two main authigenic mineral phases in the sediments, and gypsum rosettes also grow over pyrite tubes, indicating that gypsum formed after pyrite. The low $\delta^{34}S$ values of pyrite in the shallow sediment above the paleo-SMTZ are best explained by OSR. Moreover, the gypsum may be the result of the oxidation of pyrite at shallow depth. Interestingly, $\delta^{34}S$ values of pyrite increased with depth, revealing a different trend to that of gypsum. The $\delta^{34}S$ values of gypsum are lower than those of the associated pyrite in the deep sediment, because of a downward diffusion of sulfate, which resulted from the oxidation of ^{34}S depleted pyrite derived by OSR. In this case, seawater sulfate and the oxidation of pyrite derived by OSR are the two possible sources of gypsum precipitation. In addition, ^{34}S-enriched residual seawater sulfate in the deep sediment apparently played an insignificant role, probably because of its low concentration due to progressive consumption by sulfate reduction.

The increase of calcium ions in the pore water also favored precipitation of authigenic gypsum crystals. There are two sources of calcium ions for the gypsum precipitation at Core HS328. The dissolution of calcium carbonate minerals (calcite or aragonite) caused by the pyrite oxidation would result in elevated calcium ion concentrations in sediment pore water (Pierre, 2017; Lin et al., 2016c). In addition, ion exclusion during the formation of gas hydrates also would result in elevated calcium ion concentrations in a gas hydrate environment (Ussler and Paull, 1995; Wang et al., 2004; Chen et al., 2007). The low $\delta^{18}O$ values of the gypsum from active methane seeps of the southwest African Margin and South China Sea indicate that the pore water from which gypsum precipitation occurs is more or less modified by gas hydrate formation and seawater (Lin et al., 2016a; Pierre, 2017). Therefore, the calcium ions for the precipitation of gypsum come from a mixture of carbonate minerals dissolution and ion exclusion during the formation of gas hydrates.

5.4 *Evidence for methane seepage*

In natural gas hydrate or cold seep environments, enhancement of the AOM process induced by high methane fluxes from the gas hydrate dissociation at depth will leave a significant imprint in the interstitial water and the sediments (e.g., surplus hydrogen sulfide, bisulfide and iron sulfide) (e.g., Jørgensen et al.,

2004; Lim et al., 2011; Borowski et al., 2013; Chen et al., 2016; Li et al., 2016; Lin et al., 2016a, b, c, d; 2017a, b; Hu et al., 2017). For example, the enrichment of carbonate minerals has been proposed to record past seepage activity and dissolution of gas hydrates (e.g., Bayon et al., 2007, 2011; Peckmann et al., 2009; Feng et al., 2009, 2014; Han et al., 2014; Guan et al., 2016a). High concentration of sulfide has been considered an indicator of enhanced methane fluxes within the SMTZ (e.g., Jørgensen et al., 2004; Peketi et al., 2012; Borowski et al., 2013; Lin et al., 2016a, c). The enhanced fluids result in a shallow position of the SMTZ which will change the redox zonation of the sediment (Borowski et al., 1996, 1999), and AOM instead of OSR becomes the dominant process by which a favorable condition forms for the precipitation of euhedral pyrite and overgrowth of existing framboids (Fig. 5, Stage 1). The enrichment of pyrite and the higher ^{34}S values below 667 cm indicated enhanced methane fluxes which resulted in a shallower SMTZ than at present (Lim et al., 2011; Borowski et al., 2013).

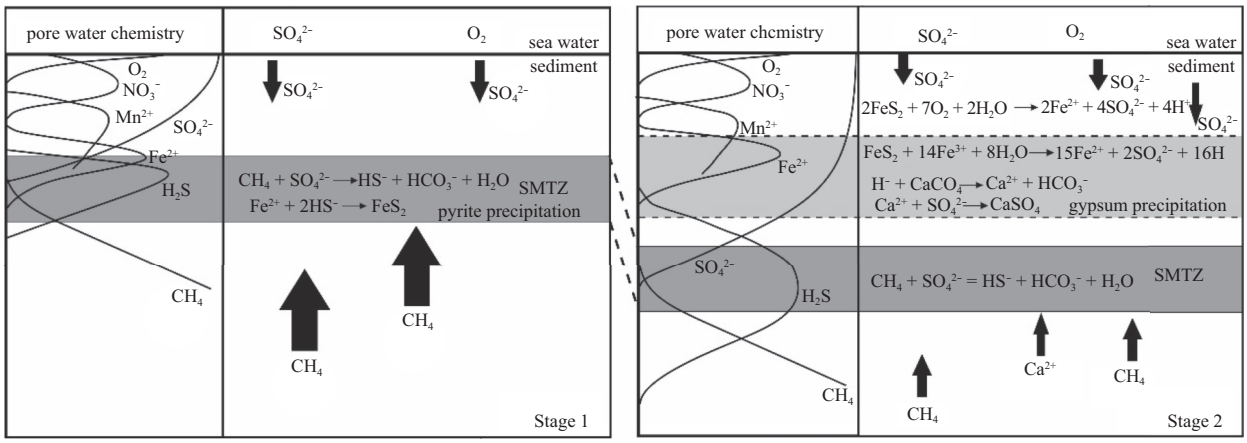

Fig. 5. Generalized schema of the formation process of authigenic pyrite and gypsum with variable seepage intensity at a site in the Shenhu area. Pore-water chemical profiles modified from Jørgensen and Kasten (2006).

When the seepage intensity is reduced, the SMTZ will shift to a greater depth, and the former anoxic environment will be changed to oxygenation through the deeper downward diffusion of seawater (Fig. 5, Stage 2, Solomon et al., 2008). The pyrite which formed in the enhanced seep time will be oxidized to sulfate using ambient electron acceptors such as iron (Ⅲ), manganese (Ⅳ) and oxygen. These additional sulfate ions probably cause dissolution of the carbonate minerals, releasing calcium ions (Pirlet et al., 2010; Pierre et al., 2012, 2017). In addition, the formation of gas hydrates also has induced elevated calcium concentrations in pore water via ion exclusion (Ussler and Paull, 1995). Therefore, we propose that the enrichment of authigenic gypsum in the paleo-SMTZ indicated variable redox conditions that were caused by variable seepage intensities in the Shenhu area and that can also be taken as evidence of enhanced methane seepage in the past.

6 Conclusions

Authigenic pyrite and gypsum are the two main minerals from the HS328 core sediment of the northern SCS. These minerals are the products of biogeochemical redox reactions in the sulfur and carbon cycle in a marine system. Bacterial sulfate reduction and sulfide oxidation are the key processes in forming these minerals. In this study, we identified the depth of the paleo-SMTZ using the occurrence of anomalously high-rich pyrites and relatively positive $^{34}S_{pyrite}$. Pyrite with a low $\delta^{34}S$ value at shallow depth predominantly formed by OSR, whereas those with a positive excursion of $\delta^{34}S$ value at great depths apparently resulted from AOM. The $\delta^{34}S$ values of gypsum varied within a narrow range (–25.0‰ to –20.7‰) and were much lower than the values of seawater sulfate. These values indicate that the dissolved sulfate from which the gypsum precipitated was caused by the oxidation of ^{34}S-depleted pyrite derived by OSR. Pyrite oxidation also promoted carbonate dissolution, resulting in increased calcium concentrations in the pore waters. In addition, ion exclusion during the formation of gas hydrates also elevated the calcium concentrations in the pore water. Therefore, authigenic pyrite and gypsum are a useful proxy for the redox conditions and seepage intensities at the study site.

Acknowledgements

The authors thank Zhang Zihu from China University of Geosciences in Wuhan and Peng Yongbo from Louisiana State University for providing the sulfur isotopic measurements and data analyses. Special thanks are also given to the Guangzhou Marine Geological Survey for providing samples and valuable suggestions.

References

Antler G, Turchyn A V, Rennie V, et al. 2013. Coupled sulfur and oxygen isotope insight into bacterial sulfate reduction in the natural environment. Geochimica et Cosmochimica Acta, 118: 98–117

Balci N, Shanks III W C, Mayer B, et al. 2007. Oxygen and sulfur isotope systematics of sulfate produced by bacterial and abiotic oxidation of pyrite. Geochimica et Cosmochimica Acta, 71(15): 3796–3811

Bayon G, Birot D, Ruffine L, et al. 2011. Evidence for intense REE scavenging at cold seeps from the Niger Delta margin. Earth and Planetary Science Letters, 312(3–4): 443–452

Bayon G, Pierre C, Etoubleau J, et al. 2007. Sr/Ca and Mg/Ca ratios in Niger Delta sediments: implications for authigenic carbonate genesis in cold seep environments. Marine Geology, 241(1–4): 93–109

Berner R A. 1980. Early Diagenesis: A Theoretical Approach. Princeton, New Jersey: Princeton University Press, 241

Boetius A, Ravenschlag K, Schubert C J, et al. 2000. A marine microbial consortium apparently mediating anaerobic oxidation of

methane. Nature, 407(6804): 623–626
Borowski W S, Paull C K, Ussler III W. 1996. Marine pore-water sulfate profiles indicate *in situ* methane flux from underlying gas hydrate. Geology, 24(7): 655–658
Borowski W S, Paull C K, Ussler III W. 1999. Global and local variations of interstitial sulfate gradients in deep-water, continental margin sediments: sensitivity to underlying methane and gas hydrates. Marine Geology, 159(1–4): 131–154
Borowski W S, Rodriguez N M, Paull C K, et al. 2013. Are ^{34}S-enriched authigenic sulfide minerals a proxy for elevated methane flux and gas hydrates in the geologic record? Marine and Petroleum Geology, 43: 381–395
Butler I B, Böttcher M E, Rickard D, et al. 2004. Sulfur isotope partitioning during experimental formation of pyrite via the polysulfide and hydrogen sulfide pathways: implications for the interpretation of sedimentary and hydrothermal pyrite isotope records. Earth and Planetary Science Letters, 228(3–4): 495–509
Butler I B, Rickard D. 2000. Framboidal pyrite formation via the oxidation of iron (II) monosulfide by hydrogen sulphide. Geochimica et Cosmochimica Acta, 64(15): 2665–2672
Böttcher M E, Thamdrup B. 2001. Anaerobic sulfide oxidation and stable isotope fractionation associated with bacterial sulfur disproportionation in the presence of MnO_2. Geochimica et Cosmochimica Acta, 65(10): 1573–1581
Böttcher M E, Thamdrup B, Gehre M, et al. 2005. ^{34}S/^{32}S and ^{18}O/^{16}O fractionation during sulfur disproportionation by *Desulfobulbus propionicus*. Geomicrobiology Journal, 25(5): 219–226
Campbell K A. 2006. Hydrocarbon seep and hydrothermal vent paleoenvironments and paleontology: past developments and future research directions. Palaeogeography, Palaeoclimatology, Palaeoecology, 232(2–4): 362–407
Canfield D E. 1991. Sulfate reduction in deep-sea sediments. American Journal of Science, 291(2): 177–188
Canfield D E, Farquhar J, Zerkle A L. 2010. High isotope fractionations during sulfate reduction in a low-sulfate euxinic ocean analog. Geology, 38(5): 415–418
Canfield D E, Thamdrup B. 1994. The production of ^{34}S-depleted sulfide during bacterial disproportionation of elemental sulfur. Science, 266(5193): 1973–1975
Chen Fang, Hu Yu, Feng Dong, et al. 2016. Evidence of intense methane seepages from molybdenum enrichments in gas hydrate-bearing sediments of the northern South China Sea. Chemical Geology, 443: 173–181
Chen Zhong, Yan Wen, Chen Muhong, et al. 2007. Formation of authigenic gypsum and pyrite assemblage and its significance to gas ventings in Nansha Trough, South China Sea. Marine Geology & Quaternary Geology (in Chinese), 27(2): 91–100
Cheng Sihai, Lu Hongfeng. 2005. Techniques for marine sediment pore-water sampling. Rock and Mineral Analysis (in Chinese), 24(2): 102–104
Deusner C, Holler T, Arnold G L, et al. 2014. Sulfur and oxygen isotope fractionation during sulfate reduction coupled to anaerobic oxidation of methane is dependent on methane concentration. Earth and Planetary Science Letters, 399: 61–73
Faure G. 1986. Principles of Isotope Geology. 2nd ed. New York: John Wiley & Sons, 1–531
Feng Dong, Birgel D, Peckmann J, et al. 2014. Time integrated variation of sources of fluids and seepage dynamics archived in authigenic carbonates from Gulf of Mexico gas hydrate seafloor observatory. Chemical Geology, 385: 129–139
Feng Dong, Chen Duofu, Peckmann J. 2009. Rare earth elements in seep carbonates as tracers of variable redox conditions at ancient hydrocarbon seeps. Terra Nova, 21(1): 49–56
Ge Lu, Jiang Shaoyong, Swennen T, et al. 2010. Chemical environment of cold seep carbonate formation on the northern continental slope of South China Sea: evidence from trace and rare earth element geochemistry. Marine Geology, 277(1–4): 21–30
Guan Hongxiang, Feng Dong, Wu Nengyou, et al. 2016a. Methane seepage intensities traced by biomarker patterns in authigenic carbonates from the South China Sea. Organic Geochemistry, 91: 109–119
Guan Hongxiang, Zhang Mei, Mao Shengyi, et al. 2016b. Methane seepage in the Shenhu area of the northern South China Sea: constraints from carbonate chimneys. Geo-Marine Letters, 36(3): 175–186
Habicht K S, Canfield D E. 2001. Isotope fractionation by sulfate-reducing natural populations and the isotopic composition of sulfide in marine sediments. Geology, 29(6): 555–558
Habicht K S, Canfield D E, Rethmeier J. 1998. Sulfur isotope fractionation during bacterial reduction and disproportionation of thiosulfate and sulfite. Geochimica et Cosmochimica Acta, 62(15): 2585–2595
Han Xiqiu, Suess E, Huang Yongyang, et al. 2008. Jiulong methane reef: microbial mediation of seep carbonates in the South China Sea. Marine Geology, 249(3-4): 243–256
Han Xiqiu, Suess E, Liebetrau V, et al. 2014. Past methane release events and environmental conditions at the upper continental slope of the South China Sea: constraints by seep carbonates. International Journal of Earth Sciences, 103(7): 1873–1887
Hu Yu, Chen Linying, Feng Dong, et al. 2017. Geochemical record of methane seepage in authigenic carbonates and surrounding host sediments: a case study from the South China Sea. Journal of Asian Earth Sciences, 138: 51–61
Jiang Shaoyong, Yang Tao, Ge Lu, et al. 2008. Geochemistry of pore waters from the Xisha Trough, northern South China Sea and their implications for gas hydrates. Journal of Oceanography, 64(3): 459–470
Jørgensen B B. 1982. Mineralization of organic matter in the sea bed-the role of sulphate reduction. Nature, 296(5858): 643–645
Jørgensen B B, Böttcher M E, Lüschen H, et al. 2004. Anaerobic methane oxidation and a deep H_2S sink generate isotopically heavy sulfides in Black Sea sediments. Geochimica et Cosmochimica Acta, 68(9): 2095–2118
Jørgensen B B, Kasten S. 2006. Sulfur cycling and methane oxidation. In: Schulz H D, Zabel M, eds. Marine Geochemistry. Berlin: Springer, 271–309
Kocherla M. 2013. Authigenic gypsum in gas-hydrate associated sediments from the east coast of India (Bay of Bengal). Acta Geologica Sinica, 87(3): 749–760
Leavitt W D, Halevy I, Bradley A S, et al. 2013. Influence of sulfate reduction rates on the Phanerozoic sulfur isotope record. Proceedings of the National Academy of Sciences of the United States of America, 110(28): 11244–11249
Li Niu, Feng Dong, Chen Linying, et al. 2016. Using sediment geochemistry to infer temporal variation of methane flux at a cold seep in the South China Sea. Marine and Petroleum Geology, 77: 835–845
Lim Y C, Lin S, Yang T F, et al. 2011. Variations of methane induced pyrite formation in the accretionary wedge sediments offshore southwestern Taiwan. Marine and Petroleum Geology, 28(10): 1829–1837
Lin Zhiyong, Sun Xiaoming, Lu Yang, et al. 2016a. Stable isotope patterns of coexisting pyrite and gypsum indicating variable methane flow at a seep site of the Shenhu area, South China Sea. Journal of Asian Earth Sciences, 123: 213–223
Lin Zhiyong, Sun Xiaoming, Lu Yang, et al. 2017a. The enrichment of heavy iron isotopes in authigenic pyrite as a possible indicator of sulfate-driven anaerobic oxidation of methane: insights from the South China Sea. Chemical Geology, 449: 15–29
Lin Zhiyong, Sun Xiaoming, Peckmann J, et al. 2016b. How sulfate-driven anaerobic oxidation of methane affects the sulfur isotopic composition of pyrite: a SIMS study from the South China Sea. Chemical Geology, 440: 26–41
Lin Zhiyong, Sun Xiaoming, Strauss, H. et al 2017b. Multiple sulfur isotope constraints on sulfate-driven anaerobic oxidation of methane: evidence from authigenic pyrite in seepage areas of the South China Sea. Geochimica et Cosmochimica Acta, 211: 153–173
Lin Qi, Wang Jiasheng, Algeo T J, et al. 2016c. Formation mechanism of authigenic gypsum in marine methane hydrate settings: evidence from the northern South China Sea. Deep-Sea Research:Part I.Oceanographic Research Papers, 115: 210–220

Lin Qi, Wang Jiasheng, Taladay K, et al. 2016d. Coupled pyrite concentration and sulfur isotopic insight into the paleo sulfate-methane transition zone (SMTZ) in the northern South China Sea. Journal of Asian Earth Sciences, 115: 547–556

Liu Changling, Ye Yuguang, Meng Qingguo, et al. 2012. The characteristics of gas hydrates recovered from Shenhu Area in the South China Sea. Marine Geology, 307–310: 22–27

Longinelli A, Flora O. 2007. Isotopic composition of gypsum samples of Permian and Triassic age from the north-eastern Italian Alps: palaeoenvironmental implications. Chemical Geology, 245(3-4): 275–284

Lu Hongfeng, Chen Fang, Liao Zhiliang, et al. 2007. Authigenic pyrite rods from the core HD196A in the north eastern South China Sea. Acta Geologica Sinica (in Chinese), 81(4): 519–525

Lu Yang, Sun Xiaoming, Lin Zhiyong. 2015. Cold seep status archived in authigenic carbonates: mineralogical and isotopic evidence from Northern South China Sea. Deep-Sea Research:Part II. Topical Studies in Oceanography, 122: 95–105

Mazumdar A, Peketi A, Joao H, et al. 2012. Sulfidization in a shallow coastal depositional setting: diagenetic and palaeoclimatic implications. Chemical Geology, 322-323: 68–78

McDonnell S L, Max M D, Cherkis N Z, et al. 2000. Tectono-sedimentary controls on the likelihood of gas hydrate occurrence near Taiwan. Marine and Petroleum Geology, 17(8): 929–936

Neretin L N, Böttcher M E, Jørgensen B B, et al. 2004. Pyritization processes and greigite formation in the advancing sulfidization front in the Upper Pleistocene sediments of the Black Sea. Geochimica et Cosmochimica Acta, 68(9): 2081–2093

Novikova S A, Shnyukov Y F, Sokol E V, et al. 2015. A methane-derived carbonate build-up at a cold seep on the Crimean slope, north-western Black Sea. Marine Geology, 363: 160–173

Ohfuji H, Rickard D. 2005. Experimental syntheses of framboids-a review. Earth-Science Reviews, 71(3–4): 147–170

Orphan V J, House C H, Hinrichs K U, et al. 2001. Methane-consuming archaea revealed by directly coupled isotopic and phylogenetic analysis. Science, 293(5529): 484–487

Peckmann J, Birgel D, Kiel S. 2009. Molecular fossils reveal fluid composition and flow intensity at a cretaceous seep. Geology, 37(9): 847–850

Peckmann J, Reimer A, Luth U, et al. 2001. Methane-derived carbonates and authigenic pyrite from the northwestern Black Sea. Marine Geology, 177(1–2): 129–150

Peketi A, Mazumdar A, Joao H M, et al. 2015. Coupled C-S-Fe geochemistry in a rapidly accumulating marine sedimentary system: diagenetic and depositional implications. Geochemistry, Geophysics, Geosystems, 16(9): 2865–2883

Peketi A, Mazumdar A, Joshi R K, et al. 2012. Tracing the paleo sulfate-methane transition zones and H_2S seepage events in marine sediments: an application of C-S-Mo systematics. Geochemistry, Geophysics, Geosystems, 13(10): Q10007

Pierre C. 2017. Origin of the authigenic gypsum and pyrite from active methane seeps of the southwest African margin. Chemical Geology, 449: 158–164

Pierre C, Bayon G, Blanc-Valleron M M, et al. 2014. Authigenic carbonates related to active seepage of methane-rich hot brines at the Cheops mud volcano, Menes caldera (Nile deep-sea fan, eastern Mediterranean Sea). Geo-Marine Letters, 34(2–3): 253–267

Pierre C, Blanc-Valleron M M, Demange J, et al. 2012. Authigenic carbonates from active methane seeps offshore southwest Africa. Geo-Marine Letters, 32(5–6): 501–513

Pirlet H, Wehrmann L M, Brunner B, et al. 2010. Diagenetic formation of gypsum and dolomite in a cold-water coral mound in the Porcupine Seabight, off Ireland. Sedimentology, 57(3): 786–805

Pirlet H, Wehrmann L M, Foubert A, et al. 2012. Unique authigenic mineral assemblages reveal different diagenetic histories in two neighbouring cold-water coral mounds on Pen Duick Escarpment, Gulf of Cadiz. Sedimentology, 59(2): 578–604

Rickard D. 2015. Pyrite: A Natural History of Fool's Gold. Oxford: Oxford University Press, : 87–116

Rickard D, Luther III G W. 2007. Chemistry of iron sulfides. Chemical Reviews, 107(2): 514–562

Sassen R, Roberts H H, Carney R, et al. 2004. Free hydrocarbon gas, gas hydrate, and authigenic minerals in chemosynthetic communities of the northern Gulf of Mexico continental slope: relation to microbial processes. Chemical Geology, 205(3–4): 195–217

Schippers A, Jørgensen B B. 2001. Oxidation of pyrite and iron sulfide by manganese dioxide in marine sediments. Geochimica et Cosmochimica Acta, 65(6): 915–922

Sim M S, Ono S, Donovan K, et al. 2011. Effect of electron donors on the fractionation of sulfur isotopes by a marine *Desulfovibrio* sp. Geochimica et Cosmochimica Acta, 75(15): 4244–4259

Solomon E A, Kastner M, Jannasch H, et al. 2008. Dynamic fluid flow and chemical fluxes associated with a seafloor gas hydrate deposit on the northern Gulf of Mexico slope. Earth and Planetary Science Letters, 270(1–2): 95–105

Suess E. 2014. Marine cold seeps and their manifestations: geological control, biogeochemical criteria and environmental conditions. International Journal of Earth Sciences, 103(7): 1889–1916

Tong Hongpeng, Feng Dong, Cheng Hai, et al. 2013. Authigenic carbonates from seeps on the northern continental slope of the South China Sea: new insights into fluid sources and geochronology. Marine and Petroleum Geology, 43: 260–271

Ussler III W, Paull C K. 1995. Effects of ion exclusion and isotopic fractionation on pore water geochemistry during gas hydrate formation and decomposition. Geo-Marine Letters, 15(1): 37–44

Wang Meng, Cai Feng, Li Qing, et al. 2015. Characteristics of authigenic pyrite and its sulfur isotopes influenced by methane seep at Core A, Site 79 of the middle Okinawa Trough. Science China: Earth Sciences, 58(12): 2145–2153

Wang Jiasheng, Suess E, Rickert D. 2004. Authigenic gypsum found in gas hydrate-associated sediments from Hydrate Ridge, the eastern North Pacific. Science in China: Series D. Earth Sciences, 47(3): 280–288

Wang Shuhong, Yan Wen, Song Haibin. 2006. Mapping the thickness of the gas hydrate stability zone in the South China Sea. Terrestrial, Atmospheric and Oceanic Sciences, 17(4): 815–828

Wegener G, Krukenberg V, Riedel D, et al. 2015. Intercellular wiring enables electron transfer between methanotrophic archaea and bacteria. Nature, 526(7574): 587–590

Wilkin R T, Barnes H L. 1996. Pyrite formation by reactions of iron monosulfides with dissolved inorganic and organic sulfur species. Geochimica et Cosmochimica Acta, 60(21): 4167–4179

Wu Nengyou, Yang Shengxiong, Zhang Haiqi, et al. 2010. Gas hydrate system of Shenhu area, northern South China Sea: wireline logging, geochemical results and preliminary resources estimates. Journal of Petroleum Technology, 62(7): 64–65

Wu Nengyou, Zhang Haiqi, Yang Shengxiong, et al. 2007. Preliminary discussion on natural gas hydrate (NGH) reservoir system of Shenhu area, north slope of South China Sea. Natural Gas Industry (in Chinese), 27(9): 1–6

Xie Lei, Wang Jiasheng, Wu Nengyou, et al. 2013. Characteristics of authigenic pyrites in shallow core sediments in the Shenhu area of the northern South China Sea: implications for a possible mud volcano environment. Science China: Earth Sciences, 56(4): 541–548

Zhang Mei, Konishi H, Xu Huifang, et al. 2014a. Morphology and formation mechanism of pyrite induced by the anaerobic oxidation of methane from the continental slope of the NE South China Sea. Journal of Asian Earth Sciences, 92: 293–301

Zhang Guangxue, Yang Shengxiong, Zhang Ming, et al. 2014b. GMGS2 expedition investigates rich and complex gas hydrate environment in the South China Sea. Fire in the Ice: Methane Hydrate Newsletter, 14(1): 1–5

Zhu Weilin, Zhong Kai, Li Youchuan, et al. 2012. Characteristics of hydrocarbon accumulation and exploration potential of the northern South China Sea deepwater basins. Chinese Science Bulletin, 57(24): 3121–3129